Journal of Magnetism and Magnetic Materials 351 (2014) 98–103

Contents lists available at ScienceDirect

Journal of Magnetism and Magnetic Materials

journal homepage: www.elsevier.com/locate/jmmm

Electronic structure, Fermi surface and optical properties of metallic compound $Be_8(B_{48})B_2$

A.H. Reshak [a,b], Sikander Azam [a,*], Z.A. Alahmed [c], Jan Chyský [d]

[a] Institute of Complex Systems, FFPW, CENAKVA, University of South Bohemia in CB, Nove Hrady 37333, Czech Republic
[b] Center of Excellence Geopolymer and Green Technology, School of Material Engineering, University Malaysia Perlis, 01007 Kangar, Perlis, Malaysia
[c] Department of Physics and Astronomy, King Saud University, Riyadh 11451, Saudi Arabia
[d] Department of Instrumentation and Control Engineering, Faculty of Mechanical Engineering, CTU in Prague, Technicka 4, 166 07 Prague 6, Czech Republic

ARTICLE INFO

Article history:
Received 11 August 2013
Received in revised form
26 September 2013
Available online 5 October 2013

Keywords:
Ceramics
Metals
Electronic structure
Fermi surface
Optical properties

ABSTRACT

The band structure, density of states, electronic charge density, Fermi surface and optical properties for $B_8(Be_{48})B_2$ compound has been investigated in the support of density functional theory (DFT). The atomic positions of $B_8(Be_{48})B_2$ compound were optimized by minimization of the forces acting on the atoms using the full potential linear augmented plane wave (FPLAPW) method. We have employed the local density approximation (LDA), generalized gradient approximation (GGA) and Engal-Vosko GGA (EVGGA) to indulgence the exchange correlation potential by solving Kohn–Sham equations. The result shows that the compound is metallic with sturdy hybridization near the Fermi energy level (E_F). The density of states at Fermi energy, $N(E_F)$, is determined by the overlaping between B-p, B-s and Be-s states. This overlaping is strong enough indicating metallic origin with different values of $N(E_F)$. These values are 16.4, 16.27 and 14.89 states/eV, and the corresponding bare linear low-temperature electronic specific heat coefficient (γ) is found to be 2.84, 2.82 and 2.58 mJ/mol K^2 for EVGGA, GGA and LDA respectively. There exists a strong hybridization between B-s and B-p states, also between B-s and Be-p states around the Fermi level. The Fermi surface is composed of three sheets. These sheets consist of set of holes and electrons. The bonding features of the compounds are analyzed using the electronic charge density in the (101 and −101) crystallographic planes and also the analyzing of charge density shows covalent bonding between B and B. The linear optical properties are also deliberated and discussed in particulars.

1. Introduction

The beryllium borides are useful ceramic materials. Innumerable investigators have recommended the continuation of at least seven stable phases in Be–B system [1–5], Be_2B, Be_4B, BeB_4, BeB_2, BeB_9, BeB_6 and BeB_{12}. Yet, the phase diagram of Be–B system has not been well established, in particular in the boron affluent region. A large amount of the Be–B compounds are thermodynamically stable and can be contrived by solid-state reaction or due to the chemical vapor deposition method.

It is thorny to achieve single crystals directly from the melt for the most boron-rich solids. High temperature solution escalation is actually a significant tool in obtaining single crystals for these compounds. Single crystals of a lot of recently originated boron-rich solids have been lucratively grown with high temperature solution technique using metal flux [6–10]. Zhang et al. [11] have achieved thin similar like plate crystals in Be–B system by means of Cu flux. The XRD measurements signify that its symmetry is tetragonal and its lattice constants are much close up to that of BeB_{12} accounted afore [12,13]. The BeB_{12} is assumed to be isostructural with MB_{25} (M=Ni, Ti, etc.). The structural scrutiny exposed that the boron icosahedral scaffold [14] in the crystal is only the same so as to in MB_{25} or $MB_{24}C$ [15–18] (M=Ni, Ti, V, etc.), but the Be position is absolutely dissimilar from M in the "old" compounds.

In this paper, we calculated the electronic structure, Fermi surface and optical properties.

The article is organized as follows: The computational method is explained in Section 2. In Section 3, first, we present the results of electronic structure, Fermi surface and optical properties. The conclusion is given in last section.

2. Crystal structure and computational method

The crystal structure of $B_8(Be_{48})B_2$ is shown in Fig. 1. The scrutinize compound has the tetragonal symmetry with space group $P4_2/nnm$ (No. 134). The lattice constant for this compound are $a=b=8.8557$ Å and $c=5.1157$ Å. The atomic positions of $B_8(Be_{48})B_2$

* Corresponding author. Tel.: +420 775928620; fax: +420 386361219.
E-mail addresses: sikander.physicst@gmail.com, sikandar_hu@yahoo.com (S. Azam).

0304-8853/$ - see front matter © 2013 Elsevier B.V. All rights reserved.
http://dx.doi.org/10.1016/j.jmmm.2013.09.060

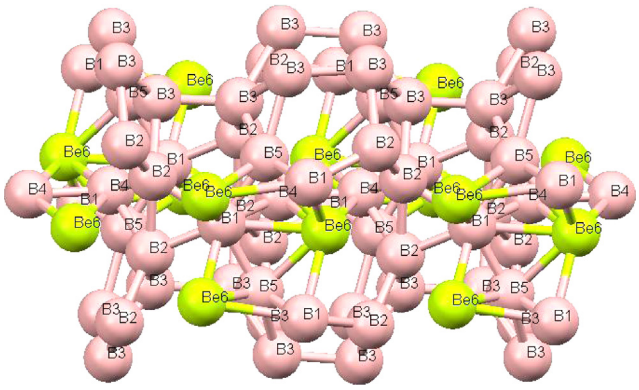

Fig. 1. Unit cell structure for $B_8(B_{48})B_2$ compound.

Table 1
Atomic coordinates ($x10^4$) and equivalent isotropic displacement parameters ($Å^2 \times 10^3$) for $Be_8(B_{48})B_2$.

Atom	X exp.	X opt.*	Y exp.	Y opt.*	Z exp.	Z opt.*
B(1)	6239(3)	6313	3761(3)	3686	1170(8)	0894
B(2)	4843(3)	4710	6665(3)	6617	1617(5)	1864
B(3)	6652(3)	6671	5774(3)	6585	1517(6)	1634
B(4)	5062(3)	5111	4938(3)	4888	3299(8)	3348
B(5)	7500	5179	2500	2500	2500	2500
Be	6546(9)	6580	3454(9)	3419	5160(20)	4991

Exp. Ref. [11].
* This work.

are given in Table 1. Highly accurate full potential linearized augmented plane wave (FPLAPW) method, as implemented in theWien2k code was used. It is based on density functional theory (DFT) [19–21]. In the present article the local density approximation (LDA), generalized gradient approximation (GGA) and Engal-Vosko GGA (EVGGA) were used to handle exchange-correction potential. In the full potential scheme the wave functions inside the muffin-tin spheres are expanded in terms of spherical harmonics up to $l_{max}=10$, and in terms of plane waves with a wave vector cutoff K_{max} in the interstitial region. RMTs are chosen in such a way that there is no charge leakage from the core and the total energy convergence is ensured. The RMT's values 1.24 and 1.58 a.u. were used for B and Be. For wave function in the interstitial region the plane wave cutoff value of $K_{max}=7$/RMT was chosen. 1000 k points were used in the irreducible Brillion zone integration. In the self consistent field for electronic structure, Fermi surface and optical properties convergence was checked through self consistency.

3. Results and discussion

3.1. Electronic structure

The optical properties are correlated to the band structure and to the probabilities of interband optical transitions. Consequently, it is of interest to evaluate the electronic structure in detail. The band structures for $Be_8(B_{48})B_2$ are presented in Fig. 2. This shows that the nature of the calculated compound is metallic as the valence and the conduction bands are found to overlap around Fermi energy. Up to our knowledge there is no tentative data on the band structure of this compound is existing in the literature to be compare with our results, so by the successful application of FP-LAPW method, we can discuss the energy band structure of the material under current study. The states around the Fermi level are due to B-p state with small admixture of B/Be-s states.

It is important to understand the nature of electrons around the Fermi surface. The density of states (DOS) at Fermi energy, $N(E_F)$, is determined by the overlaping between B-p, B-s and Be-s states. This overlaping is strong enough indicating metallic origin with different values of $N(E_F)$. These values are 16.4, 16.27 and 14.89 states/eV, for EVGGA, GGA and LDA respectively. We enlarged the band structure near E_F to show the overlapping of the bands around E_F (see Fig. 2). The electronic specific heat coefficient (γ), which is function of density of states, can be calculated using the expression,

$$\gamma = \frac{1}{3}\pi^2 N(E_F) K_\beta^2 \quad (1)$$

where $N(E_F)$ is the DOS at E_F and K_β is the Boltzmann constant. The obtained values of $N(E_F)$ enables us to calculate the bare electronic specific heat coefficient. We found that the values of bare electronic specific heat coefficient of $B_8(Be_{48})B_2$ compound are 2.84, 2.82 and 2.58 mJ/mol K^2 for EVGGA, GGA and LDA respectively.

The calculated total density of states (TDOS) and partial density of states (PDOS) for $Be_8(B_{48})B_2$ are plotted in Fig. 3. The density of states shows that boron-s states are more significant than the boron-p and beryllium-s states at lower energies i.e. between -18.0 eV and -12.0 eV. But at -12.0 eV and -3.0 eV and around the Fermi level the boron-p state is more significant than the boron/beryllium-s states. And at higher energies i.e. from 3.0 eV to 9 eV the boron-s/p states are more significant than the beryllium-s state.

There is a strong hybridization between B-s and B-p, and also between B-s and Be-p states around the Fermi level.

To visualize the chemical bonding nature between the constituents of $B_8(Be_{48})B_2$, we have calculated the distribution of charge density in the (101) plane. We plot the charge density contour in the (101) plane as illustrated in Fig. 4a. The figure shows a sharing of charge between B and B due to B-2p and B-2s hybridization, thus there is covalent bonding between B and B. The near spherical charge distribution around the boron site indicates the ionic bonding of B. In addition, we have calculated the electronic charge density in (-101) as shown in Fig. 4b. It is clear that there exists anisotropy in the electronic charge density as we move from one plane to another. Following Fig. 4a and b, we notice that the bond lengths between B and B in (101) plane is smaller than the bond lengths in (-101) plane. Our calculated bond lengths and bond angles are in good agreement with the experimental data [13] as shown in Table 2.

3.2. Fermi surface

The custody of the electronic states at the Fermi level makes clear the metallic actions of the compound. So it is important to set up the shape of the Fermi surface (FS). We have studied the FS of $B_8(Be_{48})B_2$ using the FPLAPW method as shown in Fig. 5. The calculations of $B_8(Be_{48})B_2$ exposes that there are three bands crossing Fermi level along the $R-\Gamma$ direction. The FS of $B_8(Be_{48})B_2$ compound consist of set of holes which shows the empty region and set of electrons which shows the shaded regions. In the FS the colors show the velocity of electron in which the red color shows the high velocity and the violet color shows the lowest velocity of electrons while the remaining colors have the intermediate velocity of electron. Fermi surface defines various electrons in the system, whose topology is instantly related to the transport features of materials, such as to mention electrical conductivity.

3.3. Optical properties

Further insight into the electronic structure can be obtained from the calculation of interband optical functions. The investigated

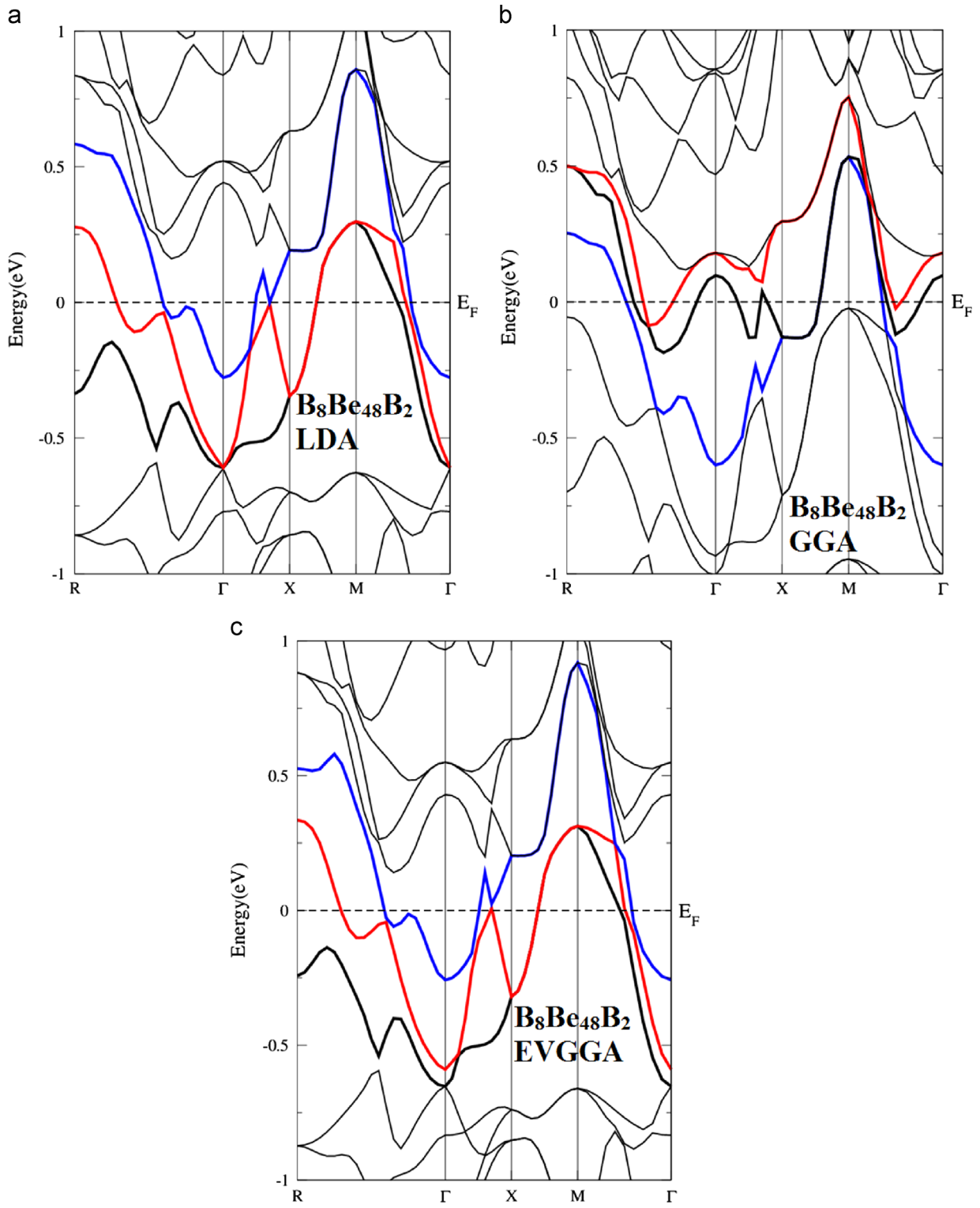

Fig. 2. Calculated band structures for LDA, GGA and EVGGA for $B_8(B_{48})B_2$ compound.

compound has the tetragonal symmetry so we resolve the optical spectra into the two principal directions, $\varepsilon^{xx}(\omega)=\varepsilon^{yy}(\omega)$ and $\varepsilon^{zz}(\omega)$. The interband transitions of the dielectric function are usually presented as a superposition of direct and indirect transitions. One can neglect the indirect interband transitions formed by electron phonon interactions that are expected to give a small contribution to $\varepsilon(\omega)$ [22].

To calculate the direct interband contributions to the imaginary part of the dielectric function $\varepsilon_2(\omega)$, we carried out summation over all possible transitions from the occupied valence to the unoccupied conduction band states. Taking the appropriate dipole interband transition matrix elements into account, we calculated the dispersion of the imaginary part of the dielectric functions $\varepsilon_2(\omega)$ using the expression [23].

$$\varepsilon_2^{ab}(\omega)=\sum_{nm}\int d\vec{k} f_{nm}\frac{\vartheta_{nm}^{\alpha}(\vec{k})\vartheta_{mn}^{\beta}(\vec{k})}{\omega_{mn}^2}\delta(\omega-\omega_{mn}(\vec{k})) \quad (2)$$

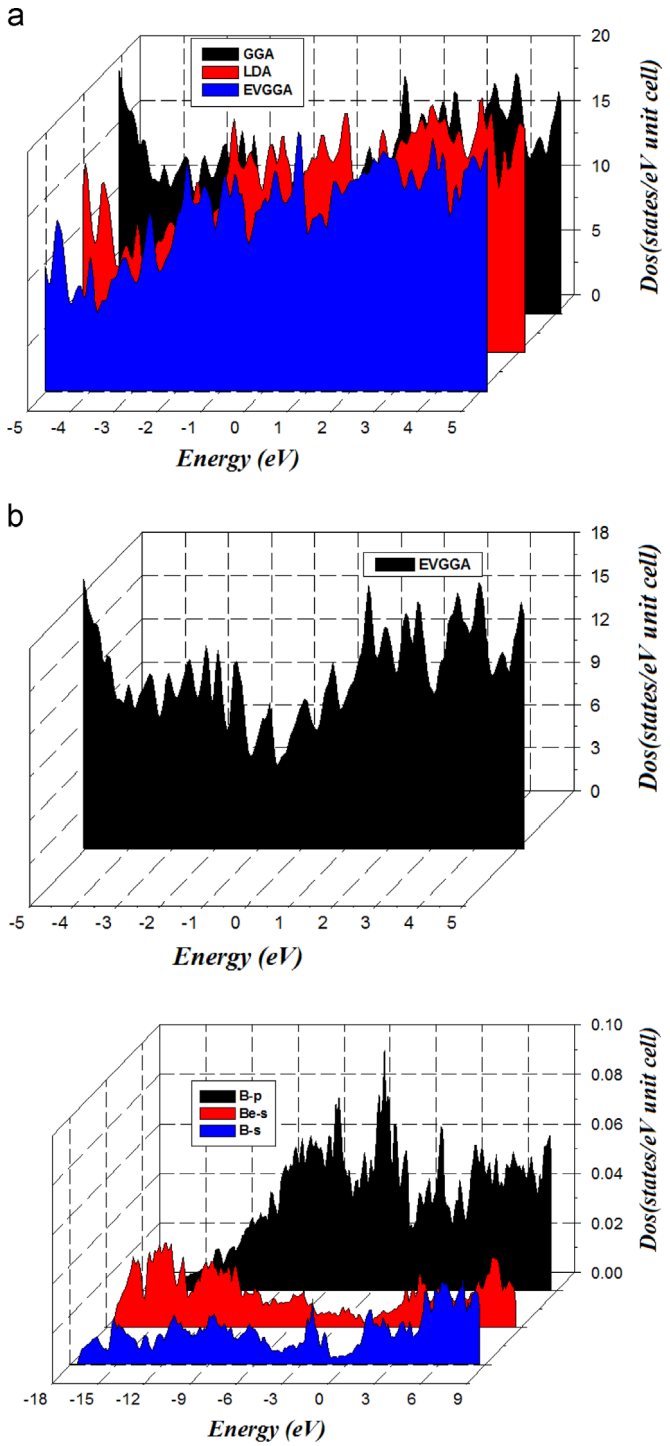

Fig. 3. Calculated total and partial density of state for $B_8(B_{48})B_2$ compound (state/eV unit cell).

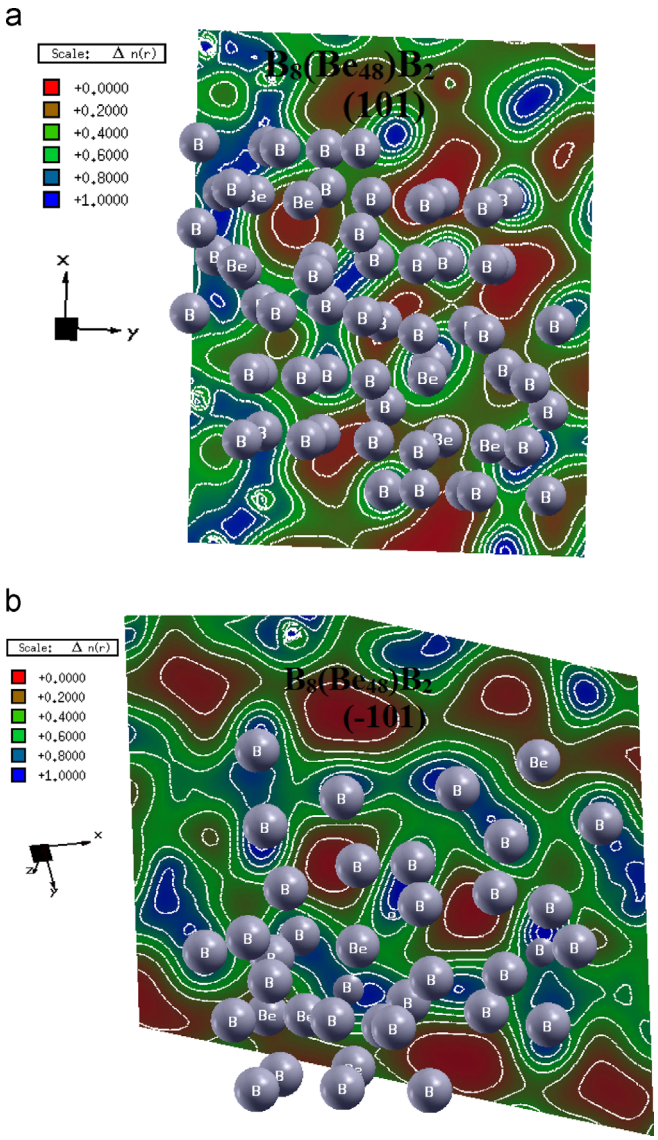

Fig. 4. Calculated Fermi surface for $B_8(B_{48})B_2$ compound.

Table 2
Selected bond lengths (Å) for $Be_8(B_{48})B_2$ compound.

Exp. theory*			Exp. theory*		
B(1)–B(2)	1.759	1.699	B(2)–B(2)	1.733(6)	1.694
B(1)–B(3)	1.828	2.953	B(3)–B(3)	1.807(6)	1.845
B(1)–B(4)	1.832	1.960	B(4)–B(4)	1.747(8)	1.713
B(2)–B(2)	1.889	1.662			
B(2)–B(3)	1.795	1.741	B(1)–B(5)	1.720(4)	1.669
B(2)–B(4)	1.766	1.745	Be–B(5)	1.809(11)	1.956
B(3)–B(3)	1.902	1.714	Be–B(1)	2.062–2.093	1.933–2.122
B(3)–B(4)	1.834	2.222	Be–B(2)	2.061–2.140	1.974–2.185
Be–B(4)	2.08–2.16	2.022–2.283	Be–Be	2.39(2)	2.303

Exp. Ref. [11].
* This work.

where ω is the photon energy and $\omega_{mn}(k)$ is the energy difference $\omega_{mn}(k)=\mathrm{Em}(k)-\mathrm{En}(k)$. The integration is performed over the first IBZ.

Fig. 6 displays the variation of the imaginary and real parts of the electronic dielectric function $\varepsilon(\omega)$. The broadening was taken to be equal to 0.1 eV [24]. The spectral peaks in the optical dispersion are caused by the allowed electric-dipole transitions between the valence and the conduction bands. In order to identify these structures we should consider the values of the optical matrix elements. The observed structures would correspond to those transitions which have large optical matrix dipole transition elements. Fig. 6a, shows the two components $\varepsilon_2^{xx}(\omega)$ and $\varepsilon_2^{zz}(\omega)$ of the imaginary part of the frequency-dependent dielectric functions. We noticed that in the imaginary part of the electronic dielectric function of $B_8(Be_{48})B_2$ there is a sharp rise for $\varepsilon_2^{xx}(\omega)$ and $\varepsilon_2^{zz}(\omega)$ below 1.0 eV. The sharp rise at low energies is due to the Drude term. The effect of the Drude term is significant for energies less than 1.0 eV. There is a considerable anisotropy between $\varepsilon_2^{xx}(\omega)$

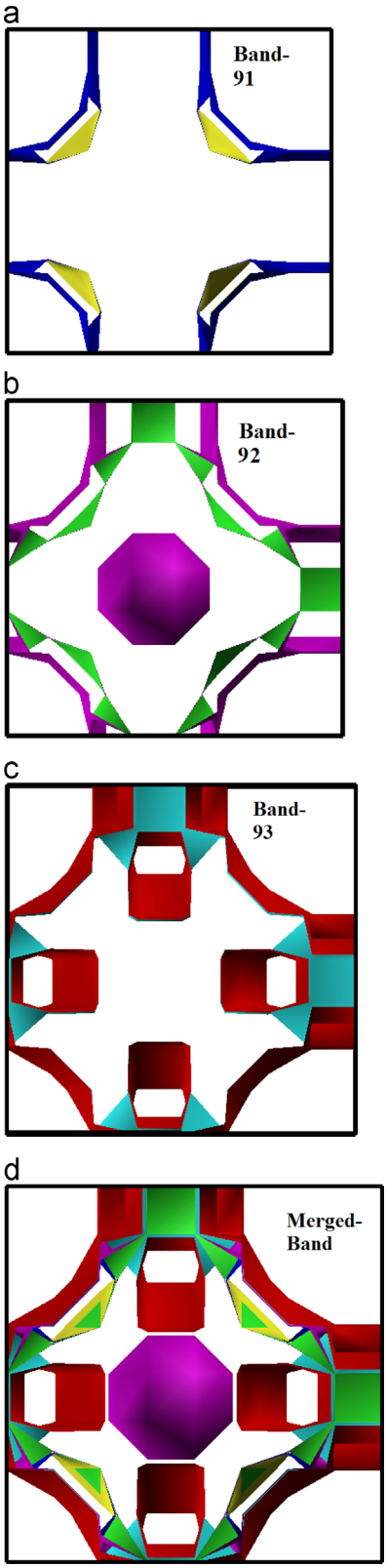

Fig. 5. Calculated electron charge density for $B_8(B_{48})B_2$ compound.

and $\varepsilon_2^{zz}(\omega)$ at the energy region between 1.0 eV and 4.0 eV, then after there exists a Clear isotropic behavior between the two components. From the imaginary parts of the dielectric function dispersions $\varepsilon_2(\omega)$ the real part $\varepsilon_1(\omega)$ can be obtained using

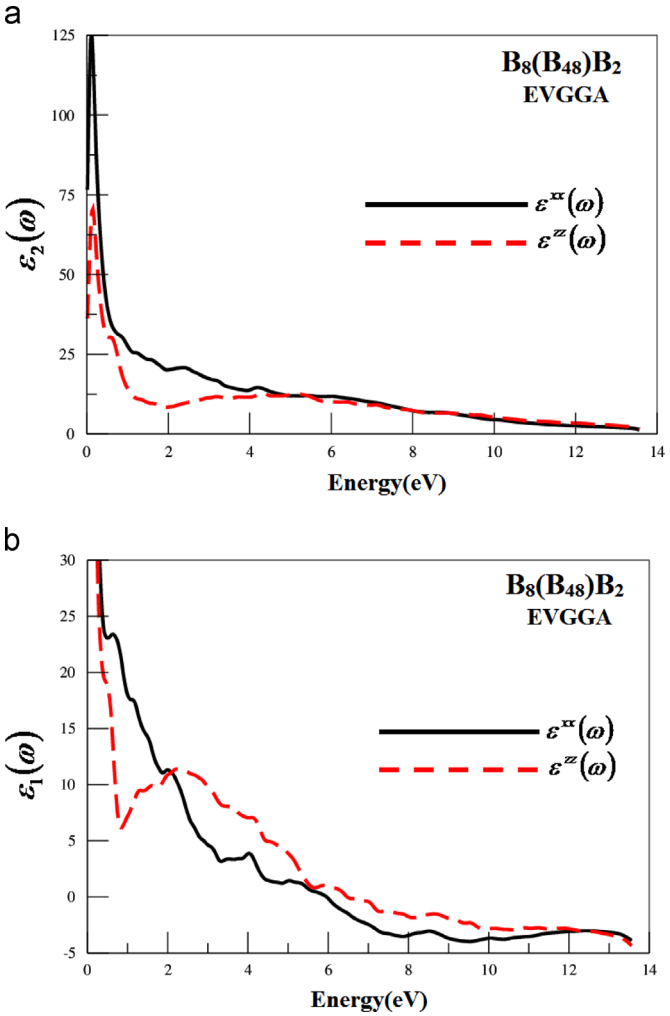

Fig. 6. Calculated imaginary part ($\varepsilon_2(\omega)$) and real part ($\varepsilon_1(\omega)$)of dielectric function for $B_8(B_{48})B_2$ compound.

Kramers–Kronig relations. The calculated components of the real part $\varepsilon_1^{xx}(\omega)$ and $\varepsilon_1^{zz}(\omega)$, show a sharp rise below 1.0 eV and considerable anisotropy between the two components along the spectral region as illustrated in Fig. 6.

4. Conclusion

We performed an exhaustive investigations on the electronic structure, electronic charge density, Fermi surface and optical properties of $B_8(Be_{48})B_2$ compound within a framework of DFT based on full potential calculations. The explored compound possesses metallic nature. The DOS at the Fermi energy (E_F) is assessed by the overlaping between B-p and B/Be-s states, with DOS at E_F, $N(E_F)$, of about 16.4, 16.27 and 14.89 states/eV for EVGGA, GGA and LDA respectively. The bare linear low-temperature electronic specific heat coefficient (γ) is found to be 2.84, 2.82 and 2.58 mJ/mol K^2 for EVGGA, GGA and LDA respectively. The bonding properties were clarified by the investigation of the electronic charge density contour in the (101) and (−101) crystallographic planes. The calculation exposes that the Fermi surface (FS) of $B_8(Be_{48})B_2$, is formed by three bands crossing along the $R-\Gamma$ direction. In the FS the colors show the velocity of electron in which the red color shows the high velocity and the violet color shows the lowest velocity of electrons while the remaining colors have the intermediate velocity of electron. The

optical dispersions, the imaginary and real parts of the dielectric function were calculated. A considerable anisotropy exists between two components of the imaginary and real parts of the electronic dielectric function. We noticed that in the imaginary and real parts of the electronic dielectric function of $B_8(Be_{48})B_2$ compound there exists a sharp rise below 1.0 eV. The sharp rise at low energies is due to the Drude term.

Aknowledegment

This work was supported from the Project CENAKVA (No. CZ.1.05/2.1.00/01.0024), the Grant no. 134/2013/Z/104020 of the Grant Agency of the University of South Bohemia. School of Material Engineering, Malaysia University of Perlis, P.O Box 77, d/a Pejabat Pos Besar, 01007 Kangar, Perlis, Malaysia. Also by the Research Center, College of Science, King Saud University.

References

[1] P. Rogl, Phase Diagram of Ternary Metal-Boron Systems, ASM International, Materials Park, OH, 1998.
[2] J. Stecher, F. Aldinger, Zeitschrift für Metallkunde 64 (1973) 684.
[3] K. Krogmann, H.J. Becher, Zeitschrift fuer Anorganische und Allgemeine Chemie 392 (1972) 197.
[4] J.B. Holt, Journal of the American Ceramic Society 57 (1974) 126.
[5] I. Higashi, Journal of Solid State Chemistry 32 (1980) 201.
[6] F.X. Zhang, F.X. Xu, A. Leithe-Jasper, T. Mori, T. Tanaka, A. Sato, P. Salamakha, Y. Bando, Journal of Alloys and Compounds 337 (2002) 120.
[7] F.X. Zhang, F.F. Xu, Z. Leithe-Jasper, T. Mori, T. Tanaka, J. Xu, A. Sato, Y. Bando, Y. Matsui, Inorganic Chemistry 40 (2001) 6948.
[8] F.X. Zhang, F.F. Xu, T. Mori, Q.L. Liu, A. Sato, T. Tanaka, Journal of Alloys and Compounds 329 (2001) 168.
[9] F.X. Zhang, A. Sato, T. Tanaka, Journal of Solid State Chemistry 164 (2002) 361.
[10] F.X. Zhang, F.X. Xu, T. Mori, Q.L. Liu, T. Tanaka, Journal of Solid State Chemistry 170 (2003) 75.
[11] F.X. Zhang, et al., Journal of Solid State Chemistry 177 (2004) 3070–3074.
[12] H.J. Becher, Zeitschrift fuer Anorganische und Allgemeine Chemie 306 (1960) 266.
[13] I. Higashi, Journal of Crystal Growth 128 (1993) 1113.
[14] F.X. Zhang, F.F. Xu, T. Tanaka, Journal of Solid State Chemistry 177 (2004) 3070–3074.
[15] E. Amberger, K. Polborn, Acta Crystallographica B 31 (1975) 949.
[16] E. Amberger, K. Polborn, Acta Crystallographica B 36 (1980) 672.
[17] K. Ploog, Acta Crystallographica B 32 (1976) 981.
[18] B.F. Decker, J.S. Kasper, Acta Crystallographica 13 (1960) 1030.
[19] P. Hohenberg, W. Kohn, Physical Review B 136 (1964) 864;
W. Kohn, L.J. Sham, Physical Review A 140 (1965) 1133.
[20] W. Wimmer, H. Krakauer, M. Weinert, A.J. Freeman, Physical Review B 24 (1981) 864.
[21] P. Blaha, K. Schwarz, G.K.H. Madsen, D. Kvasnicka, J. Luitz, Wien2k An Augmented Plane Wave Plus Local Orbital Program for Calculating the Crystal Properties, in: Karlhein Schwarz (Ed.), Vienna University of Technology, Austria, 2001.
[22] N.V. Smith, Physical Review B 3 (1862) 1971.
[23] M.A. Khan, A.K. Arti Kashyap, T. Solanki, S.Auluck Nautiyal, Physical Review B 23 (1993) 16974.
[24] A.H. Reshak, X. Chen, S. Auluck, I.V. Kityk, Journal of Chemical Physics 129 (2008) 204111.